nature neuroscience

ARTICLES

MPS-1 is a K^+ channel β-subunit and a serine/threonine kinase

Shi-Qing Cai, Leonardo Hernandez, Yi Wang, Ki Ho Park & Federico Sesti[1]

We report the first example of a K^+ channel β-subunit that is also a serine/threonine kinase. MPS-1 is a single–transmembrane domain protein that coassembles with voltage-gated K^+ channel KVS-1 in the nervous system of the nematode *Caenorhabditis elegans*. Biochemical analysis shows that MPS-1 can phosphorylate KVS-1 and other substrates. Electrophysiological analysis in Chinese hamster ovary (CHO) cells demonstrates that MPS-1 activity leads to a significant decrease in the macroscopic current. Single-channel analysis and biotinylation assays indicate that MPS-1 reduces the macroscopic current by lowering the open probability of the channel. These data are consistent with a model that predicts that the MPS-1–dependent phosphorylation of KVS-1 sustains cell excitability by controlling K^+ flux.

Potassium (K^+) channels are an important class of integral membrane proteins that control the resting membrane potential and excitability of biological cells. K^+ channels are tetramers composed of four identical subunits, packed around a water-filled pore[1,2]. This simple homomeric structure is sufficient to give rise to functional channels, but it is observed only sporadically in nature. Often, K^+ channels require additional regulatory proteins, such as β-subunits, to fine-tune their trafficking to the plasma membrane, their location and abundance, their sensitivity to stimulation and their pharmacology. KCNE proteins are a class of β-subunits of voltage-gated K^+ channels[3–7] that have been conserved through evolution. These subunits are integral membrane proteins[8] and, by virtue of this characteristic, are able to interact intimately with the channel[9–11] to affect several functional properties[12–15]: namely, to control how signaling molecules modulate the channel[16,17], to partner with multiple channels[4,18] and to cause congenital and acquired channelopathies[19–24].

Signaling molecules such as protein kinases also have a central role in the modulation of K^+ channels. Protein kinases are among the largest and most heterogeneous families of proteins in eukaryotes; they regulate innumerable biological processes including metabolism, transcription, cell cycle progression, cytoskeletal rearrangement and cell movement, and apoptosis and differentiation. Protein phosphorylation is also critical in intercellular communication during development, in physiological response and homeostasis, and in the functioning of the nervous and immune systems[25]. Even though both protein kinases and β-subunits act to alter the function of channels and, ultimately, the electrical activities of the cell, the molecular basis for the way in which they function, and the effects they produce, are fundamentally different. Accessory subunits form stable complexes with channels and therefore cause permanent modifications by passively changing the three-dimensional structure of the complex, its amino acid content, or both. In contrast, protein kinases produce reversible alterations by actively catalyzing the incorporation, into the target protein, of phosphates that can be removed by phosphatases.

In this paper we report an example of a K^+ channel β-subunit that is also a serine/threonine kinase. MPS-1 was originally cloned during the process of identifying *C. elegans* orthologs of human KCNE proteins[26]. MPS-1 forms a channel complex with the voltage-gated K^+ channel KVS-1 in the nervous system of the nematode[6,26]. When expression of the *MPS-1* gene is reduced by RNA interference (RNAi), the animals show several sensory defects, thus emphasizing the important physiological roles of this K^+ channel and of MPS-1 (ref. 26). Here we show that MPS-1 is able to control KVS-1 activity through independent mechanisms that stem from its dual role—as β-subunit and protein kinase.

RESULTS

MPS-1 has kinase activity

The amino acid sequence of MPS-1 contains two characteristic protein kinase motifs: a DFG (AspPheGly) triplet, which identifies the Mg^{2+} binding site of ATP molecules, and a HisSerAsp (HSD) triplet that can have catalytic function (**Fig. 1**), which suggests that MPS-1 might be a kinase[25]. To test the hypothesis that MPS-1 is a kinase, we expressed histidine-tagged wild-type *MPS-1* in *Escherichia coli*, along with a putatively inactive variant bearing a mutation that causes a D178N amino acid substitution in the DFG catalytic site. We purified the recombinant proteins by immobilized metal ion affinity chromatography and evaluated their enzymatic activity in kinase assays. In the insoluble fraction of *E. coli* lysates, antibodies to histidine detected the full-length protein (~35 kDa) as well as a fragment migrating at approximately the 16-kDa position (wild type, **Fig. 2a**; data for the D178N mutant not shown) that was still present after purification

University of Medicine and Dentistry of New Jersey, Robert Wood Johnson Medical School, Department of Physiology and Biophysics, 683 Hoes Lane, Piscataway, New Jersey 08854, USA. [1]Correspondence should be addressed to F.S. (sestife@umdnj.edu).

Received 15 August; accepted 2 September; published online 16 October 2005; doi:10.1038/nn1557

```
MHKNISPTCQEGIREACITLKNACDPQVLDKAAIRMR   35
EYENEFGRILYTISILIMFSFVIILLMVRSIRRTQST   70
VEMDSLLDAMRIREELEIQERKRRRLMRAKTQVTAWL  105
VNKNKEKGPEKRKDSEWKPLPNGTRPRGHYSISTVTS  140
DIPEIVVSADDCIHSDFPNRPHTPAISMIYDFGIASP  175
DLIEPDSRKPSISSSTAIPMSSSSSSSMNSLIEPNMN  210
SIKSNPRTYSLDTNASTSSRTPRVDCDDKSFSLDV    243
```

Figure 1 MPS-1 shows characteristic protein kinase motifs. Amino acid sequence of MPS-1. The transmembrane domain and the motifs thought to be critical for catalytic function are in bold. DFG is well conserved among kinases and it chelates the Mg^{2+} ions of ATP. The aspartate of the HRD triplet (modified to HSD) can be catalytic by acting as a base acceptor.

(as shown in the Coomassie blue–stained blot in **Fig. 2b**). The antibodies did not detect any protein in the solubilized fraction (data not shown), suggesting that the fragment is a proteolytic cleavage product of MPS-1 that retains the N-terminus and the transmembrane span but lacks the catalytic domain. To test for MPS-1 kinase activity, we carried out enzymatic reactions using myelin basic protein (MBP) as a test substrate, and found that wild-type, but not D178N, *MPS-1* catalyzed the incorporation of ^{32}P into MBP (**Fig. 2c**). Moreover, incorporation of the phosphate could be inhibited by the generic kinase inhibitor staurosporine (10 μM) and partially reversed by calf intestinal alkaline phosphatase in imidazole-free conditions (**Fig. 2d–e**). The lack of activity in the mutant confirmed that the proteolytic cleavage product was enzymatically inactive and ruled out the possibility that kinases other than MPS-1 might phosphorylate MBP—a result that was not unexpected given that *E. coli* does not have endogenous serine/threonine kinases. To obtain a rough estimate of the ability of MPS-1 to phosphorylate MBP, we compared its activity to that of bovine protein kinase A (PKA), whose interaction with MBP has been extensively investigated[27,28]. By quantifying the bands on the autoradiogram by densitometric analysis using Gel-Doc software (Bio-Rad), we estimated that MPS-1 phosphorylates MBP approximately 20 times less efficiently than does PKA (data not shown). This low activity is not unusual[29,30] and could be caused by several factors, including the relative impurity of the preparation and the fact that MBP is not a physiological substrate for MPS-1. The time course of phosphorylation of MBP by MPS-1 (**Fig. 2f**) showed that, as with other kinases[31,32], the incorporation of ^{32}P into MBP increased during the first ~15 min and then saturated.

We next assessed MPS-1–mediated phosphorylation of MBP by using rabbit antibodies to phosphoserine and phosphothreonine (anti-pS/pT) that have been shown to produce very specific immunological reactions[33]. The rationale for these experiments was twofold: first, to provide an independent line of evidence in support of the notion that MPS-1 is a kinase; and second, to test the reagents that were used to determine the phosphorylation of an MPS-1 substrate in the CHO cell expression system (see below). As expected, staining with anti-pS/pT showed that a significantly greater MBP phosphorylation occurred when MPS-1 was present (**Fig. 3**). The antibodies also detected phosphorylated residues in MPS-1, suggesting that MPS-1 might autophosphorylate—a common feature of protein kinases[34]. The fact that we did not observe the incorporation of ^{32}P into MPS-1 (**Fig. 2**) might indicate that purified MPS-1 is phosphorylated in *E. coli*, a relatively frequent occurrence[35].

K^+ channel KVS-1 is a physiological substrate for MPS-1

We next asked whether the K^+ channel KVS-1 is a substrate for MPS-1, as the two proteins form stable and functional complexes in native cells[6,26]. To evaluate KVS-1 phosphorylation biochemically, we used a construct, *KVS-1–HA*, encoding KVS-1 with the hemagglutinin (HA) epitope tag attached to its C terminus. This epitope tagging had no effect on the macroscopic channel activity (data not shown). In a typical experiment, KVS-1–HA subunits were expressed, alone or with MPS-1, in CHO cells (**Fig. 4a**); KVS-1 was immunoprecipitated, and protein levels were evaluated by Coomassie staining and then western blotting using antibodies to HA. The same blot was then thoroughly washed and re-stained with anti-pS/pT. Although the amounts of KVS-1 protein were similar in both lanes, anti-pS/pT staining was significantly greater in the MPS-1 + KVS-1–HA lane (**Fig. 4a**); this effect was suppressed by preincubation with staurosporine (**Fig. 4b**). In a few experiments, KVS-1 alone yielded a faint band (see, for example, **Fig. 4c**), an effect we ascribe to the action of endogenous kinases. Deleting the entire MPS-1 C terminus, by introducing a stop sequence at position 132 (ΔMPS-1; **Fig. 4c**), or inactivating the DFG catalytic site (**Fig. 4c**) was sufficient to suppress the MPS-1–mediated phosphorylation of KVS-1. To exclude the possibility that the lack of phosphorylation could be due to defective coassembly, we co-immunoprecipitated KVS-1 and MPS-1 subunits tagged with c-Myc at the C terminus (the tag had no effect on the macroscopic channel activity; data not shown). As expected, both wild-type and mutant MPS-1 subunits formed stable complexes with KVS-1 in CHO cells (**Fig. 4d**). Taken together, these data led us to conclude that MPS-1 is the first example of a K^+ channel β-subunit that is also a protein kinase.

MPS-1 activity decreases the macroscopic K^+ current

In CHO cells, KVS-1 subunits generated robust K^+ currents characterized by an A-type profile (**Fig. 5a**). Coexpression with MPS-1

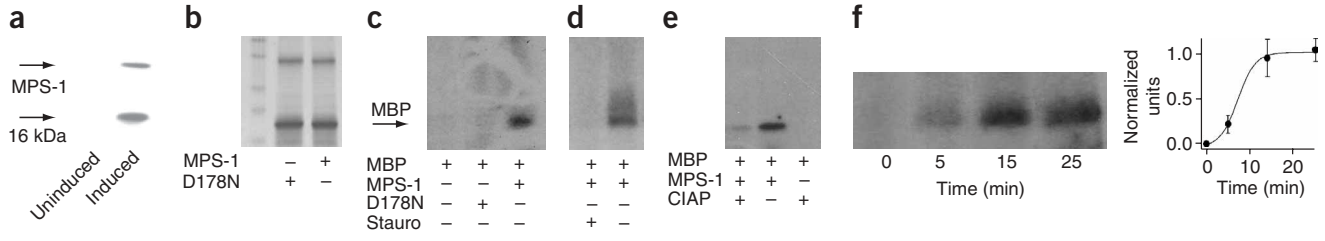

Figure 2 MPS-1 phosphorylates MBP *in vitro*. (**a**) Western blot visualization, using antibodies to histidine, of recombinant histidine-tagged MPS-1 (arrow) from insoluble fractions of *E. coli* lysates. The lower band is an MPS-1 proteolytic cleavage. (**b**) Coomassie staining of purified D178N and wild-type (MPS-1) proteins. (**c**) Autoradiogram of phosphorylation reactions carried out in the presence of [γ-^{32}P]ATP and ~3 μg of each indicated protein. (**d**) As in **c**, with and without 10 μM staurosporine included in the reaction. (**e**) As in **c**, with and without 20 units of CIAP in imidazole-free solutions. The faint band in the first lane is probably due to residual traces of imidazole, an inhibitor of CIAP. (**f**) Time course of MBP phosphorylation by MPS-1, as quantified by densitometric analysis ($n = 2$).

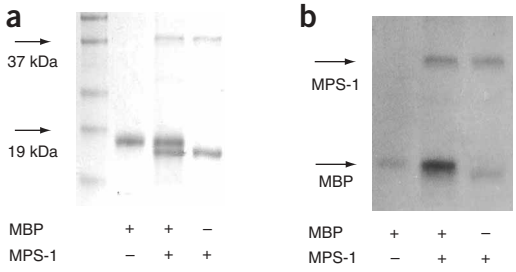

Figure 3 MPS-1 activity can be detected by antibodies to phosphoserine and phosphothreonine (anti-pS/pT). (**a**) Coomassie staining of protein content of typical kinase reactions with the indicated proteins. The marker is BenchMark (Invitrogen). (**b**) Western blot visualization of the same sample gel with anti-pS/pT.

introduced several modifications in the current (**Fig. 5**), including decreased macroscopic current density (**Fig. 5a–b**), speeded inactivation kinetics (**Fig. 5d**), a leftward shift in the midpoint for activation, slower recovery from inactivation and increased susceptibility to 4-aminopyridine[26]. To assess whether some of these effects were due to the phosphorylation of KVS-1, we electrophysiologically characterized channel complexes composed of KVS-1 alone and of KVS-1 with wild-type MPS-1, D178N or ΔMPS-1. In both mutants, the magnitude of the current density was restored to values similar to those seen with KVS-1 subunits (**Fig. 5b**). In contrast, the inactivation kinetics (**Fig. 5d**), voltage activation and recovery from inactivation (data not shown) of the mutants were not substantially different from those of the channels formed with wild-type subunits. To corroborate the notion that MPS-1 kinase activity modulates the magnitude of the current density, we treated with staurosporine cells that expressed either KVS-1 channels or KVS-1–MPS-1 channels. Although preincubation with 2 μM staurosporine did not modify the characteristics of the KVS-1 channels, it led to an approximately twofold increase in the magnitude of the current produced by KVS-1–MPS-1 channels (**Fig. 5b**). When staurosporine was dialyzed into the cell from the patch pipette solution, the current increased sigmoidally for about 15 min and then saturated—probably owing to an incomplete diffusion of staurosporine in the narrowest part of the pipette (**Fig. 5c**). Moreover, staurosporine had no effect on inactivation kinetics (**Fig. 5d**), voltage activation or recovery from inactivation (data not shown) in either the homomeric KVS-1 or the heteromeric KVS-1–MPS-1 channels.

MPS-1 activity decreases the open probability

MPS-1 might decrease the macroscopic current of the complex through distinct mechanisms. For instance, phosphorylation might alter the unitary attributes of the channel or, alternatively, its expression in the plasma membrane. To distinguish between these possibilities, we used the on-cell configuration of the patch clamp to study the properties of single KVS-1 channels under three conditions: alone, with wild-type MPS-1 and with ΔMPS-1. Consistent with macroscopic inactivation, cell depolarization evoked transient single-channel activity characterized by brief, irregular channel opening (**Fig. 6a**) that subsided after a few milliseconds. Ensemble histograms constructed by summing between 100 and 300 individual traces showed that the inactivating currents could be fitted to a single exponential (**Fig. 6b**): the time course of inactivation, τ, for the KVS-1, KVS-1–MPS-1 and KVS-1–ΔMPS-1 channels were, respectively, 35 ± 11 ms (mean ± s.e.m.) ($n = 3$), 17 ± 7 ms ($n = 3$) and 21 ± 9 ms ($n = 2$)—in good agreement with whole-cell data. The unitary slope conductance (**Fig. 6c**) of the KVS-1–MPS-1 and KVS-1–ΔMPS-1 channels ($\gamma = 19 \pm 3$ pS and $\gamma = 20 \pm 2$ pS, respectively) was not substantially different from that of the KVS-1 channel ($\gamma = 17 \pm 2$ pS); this ruled out the possibility that MPS-1–dependent phosphorylation affects the permeation of K^+.

We next tested the possibility that MPS-1 might affect surface expression. Accordingly, we incubated cells transfected with *KVS-1* alone or with *KVS-1* and *MPS-1* or mock transfected with a membrane-impermeant biotin analog; we then precipitated extracts using streptavidin-agarose beads and estimated the amount of protein in the gel by densitometric analysis. The results of these experiments indicated that MPS-1 neither decreased nor increased the number of KVS-1 channels in the plasma membrane (a representative gel is shown in **Fig. 6d**): in fact, we estimated that the ratio of KVS-1 channels to KVS-1–MPS-1 channels was 0.9 ± 0.1 ($n = 3$; data not shown). Similarly, MPS-1 neither increased nor decreased the total amount of KVS-1 protein that was detected upon Coomassie staining (data not shown). These results led us to conclude that MPS-1–dependent phosphorylation decreases the open probability. To evaluate this quantity, we idealized single-channel transitions and estimated the dwell-closed and dwell-open times. Both open- and closed-time distributions were well fit by two exponential components. Consistent with their

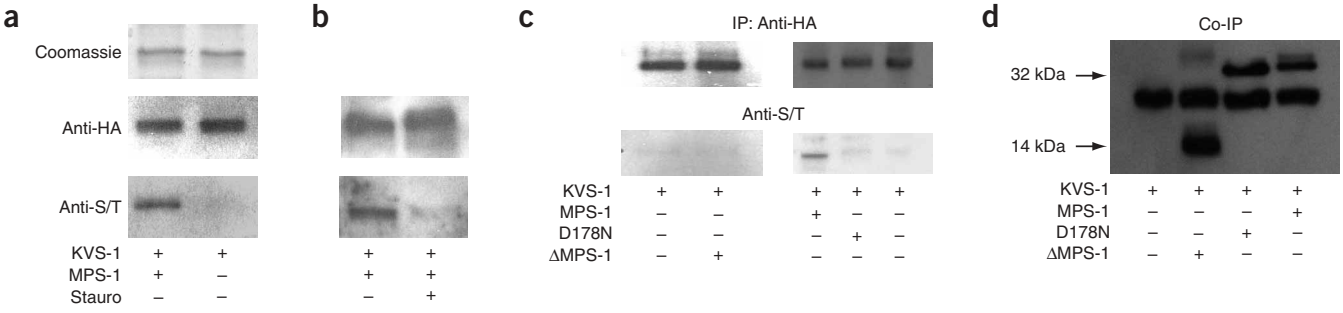

Figure 4 MPS-1 phosphorylates KVS-1 in CHO cells. (**a**) Coomassie stain (top) and western blot visualization of immunoprecipitates (IP, with antibody to HA; middle) of HA epitope–tagged KVS-1 subunits with MPS-1 and alone. The membrane was washed and re-stained with rabbit antibodies to phosphoserine and phosphothreonine (anti-pS/pT; bottom). MPS-1 yielded a more intense band that could not be attributed to differences in protein levels. (**b**) Western blot visualizations as in **a**, for CHO cells co-transfected with *MPS-1* and *KVS-1* cDNA; not incubated (left) or preincubated with 2 μM staurosporine for 45 min (right). (**c**) Western blot visualizations as in **a** for the indicated proteins. (**d**) Co-immunoprecipitations of KVS-1–ΔMPS-1 (~14 kDa band), D178N–KVS-1 and KVS-1–MPS-1 (~32-kDa bands) channels. KVS-1 channels alone did not yield any band. The band around 25 kDa is the light chain of the antibody to hemagglutinin conjugated to the matrix.

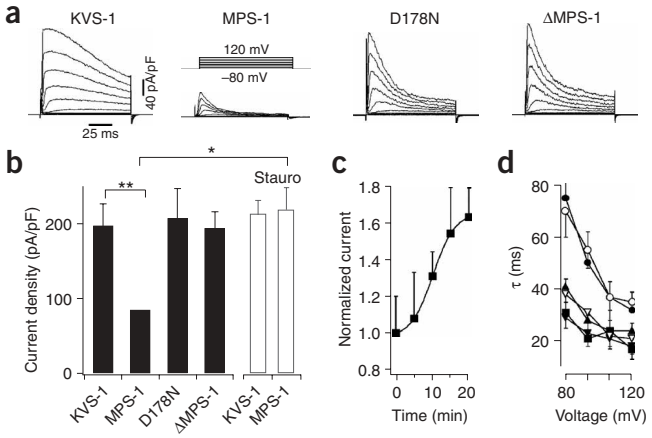

Figure 5 MPS-1 kinase activity decreases the macroscopic current. (**a**) Whole-cell macroscopic currents generated by voltage jumps from –80 mV to +120 mV in 20 mV increments (voltage protocol shown above graph for MPS-1), in CHO cells expressing *KVS-1* alone or with wild-type(MPS-1), D178N or ΔMPS-1. (**b**) Macroscopic current densities calculated by normalizing the peak current at +120 mV to the cell capacitance (filled bars; $n \geq 20$ cells for each bar). Unshaded bars indicate current densities in the presence of 2 μM staurosporine from cells preincubated for 30 min with 2 μM staurosporine (left unshaded bar: $n = 10$ cells; right unshaded bar: $n = 11$ cells). Error bars represent s.e.m. Asterisks indicate significant differences in current densities (*, $P < 0.05$; **, $P < 0.01$; *t*-test). (**c**) Time course of staurosporine-dependent current increase of the KVS-1–MPS-1 channels. The current was normalized to its value at $t = 0$—the time at which the whole-cell configuration was established. Cells were not preincubated with staurosporine. $n = 3$ cells. (**d**) Inactivation rates for the KVS-1 (●, $n = 19$), KVS-1–MPS-1 (▼, $n = 22$), KVS-1–D178N (■, $n = 13$) and KVS-1–ΔMPS-1 (▲, $n = 12$) channels and for the KVS-1 (○, $n = 10$) and KVS-1–MPS-1, ▽, $n = 11$) channels with 2-μM staurosporine. Time constants were obtained by fitting the macroscopic currents to a single exponential function: $I_0 + I_1\exp(-t/\tau)$.

faster inactivation kinetics, heteromeric (that is, KVS-1–MPS-1) channels had shorter mean open times than did KVS-1 channels; in contrast, coexpression with wild-type—but not ΔMPS-1—resulted in a roughly two-fold increase in dwell time in the long closed state (**Table 1**). Thus, shorter open times coupled with longer closed times are expected to decrease the open probability of the channel and, consequently, the macroscopic current. Because of the flickering behavior of these channels, we also used nonstationary noise variance analysis[36] to obtain an independent estimate of the unitary current *i* and the open probability p_o. Representative experiments show (**Fig. 7**) that although the estimated values of the unitary current were similar for both the KVS-1 and KVS-1–MPS-1 channel types ($i = 0.78 \pm 0.09$ pA and $i = 0.74 \pm 0.07$ pA, respectively; $n = 3$), the estimated open probability for the KVS-1 channel was about twice that of the KVS-1–MPS-1 channel ($p_o = 0.63 \pm 0.07$ and $p_o = 0.30 \pm 0.06$, respectively). Thus we conclude that the kinase activity of MPS-1 decreases the open probability of the complex.

DISCUSSION

We report here the identification of a K^+ channel β-subunit with kinase properties. Using ^{32}P-radiolabeling and immunochemical methods, we found that MPS-1 can phosphorylate the classic test substrate MBP *in vitro*. Further, another set of immunochemical tests showed that in mammalian cells, MPS-1 assembles with and phosphorylates its physiological substrate, the K^+ channel KVS-1. Notably, MPS-1 does not show sequence homologies to conventional kinases, yet it has two conserved motifs, including a DFG triplet. The fact that the aspartate in the DFG site is replaced with asparagine and that staurosporine inhibits the catalytic activity of the protein suggest that MPS-1 might operate through conventional mechanisms. In fact, sequence homology is not a prerequisite for kinase function—α-kinases, a recently discovered family[37] that includes channel-kinases[38,39], show no detectable sequence homologies to conventional protein kinases; yet the majority of structural elements, sequence motifs and the position of key amino acid residues important for catalysis appear to be remarkably conserved[39]. The bifunctional nature of MPS-1 is emphasized by the observation that the inactivation or deletion of the catalytic domain

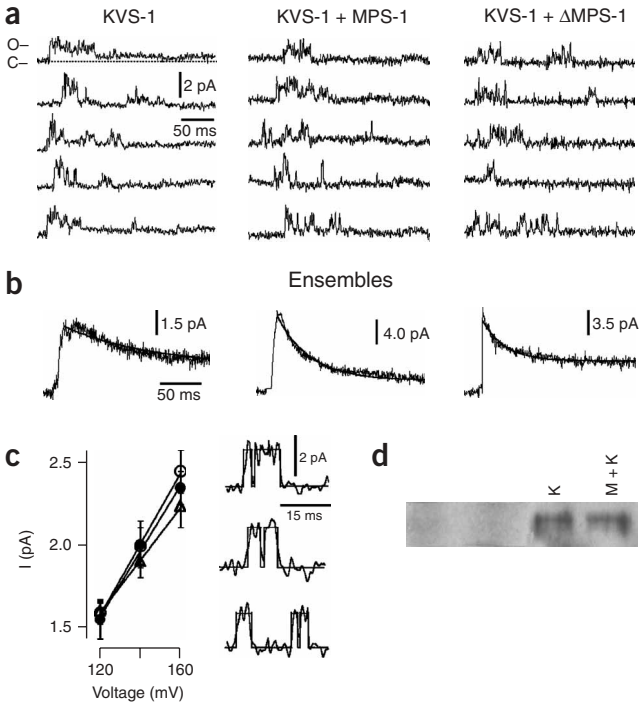

Figure 6 MPS-1 decreases the open probability of the KVS-1 channel. Between 50 and 300 depolarizing voltage jumps, each lasting 2–5 s, were applied consecutively (with a 1-s–long interpulse interval) so as to raise the channel voltage from –80 mV to +140 mV. The capacitative transient was eliminated by subtracting out each single trace from an ensemble of traces with no activity. (**a**) Representative recordings of the activity in the KVS-1, KVS-1–MPS-1 and KVS-1–ΔMPS-1 channels, in CHO cells at +140 mV. Closed (c-) and open (o-) states are indicated. For display purposes, the data were digitally filtered at 0.5 kHz. (**b**) Representative ensemble histograms of the same channels at +140 mV. The histograms were constructed by averaging 100 (KVS-1), 300 (KVS-1–MPS-1) and 200 (KVS-1–ΔMPS-1) traces. For each channel, the data were fitted to a single exponential ($\tau = 38$ ms, $\tau = 19$ ms and $\tau = 26$ ms, respectively). (**c**) *i-V* characteristics of KVS-1 (●), KVS-1–MPS-1 (○) and KVS-1–ΔMPS-1 channels (△). Each data point represents the average of two or three patches. Inset, representative idealized single-channel transitions. Top to bottom, KVS-1 channels alone, KVS-1–MPS-1 and KVS-1–ΔMPS-1. (**d**) Surface expression of KVS-1 and KVS-1–MPS-1 channels in CHO cells. First lane, mock-transfected cells. Second lane, cells transfected with *KVS-1–HA* but not incubated with the biotin analog. Third and fourth lanes: cells transfected, respectively, with *KVS-1–HA* (K) and with *KVS-1–HA* and *MPS-1* (K+M). Western blot visualization was performed with a monoclonal antibody to HA; for fluorography, chemiluminescence was performed with a secondary antibody coupled to horseradish peroxidase.

Table 1 First latency and time constants of open and closed states of KVS-1, KVS-1–MPS-1 and KVS-1–ΔMPS-1 channels

	Open times				Closed times		
Channel	1st lat., ms	$A_2/(A_1+A_2)$	τ_{o1}, ms	τ_{o2}, ms	$A_2/(A_1+A_2)$	τ_{c1}, ms	τ_{c1}, ms
KVS-1 ($n = 7$)	2.7 ± 1.3	0.06 ± 0.01	0.6 ± 0.1	5.5 ± 1.6	0.36 ± 0.1	3.0 ± 0.4	11.4 ± 1.6
MPS-1/KVS-1 ($n = 6$)	4.6 ± 2.4	0.14 ± 0.06 (**)	0.7 ± 0.1	2.7 ± 0.2 (*)	0.32 ± 0.1	3.3 ± 0.8	25.1 ± 5.5 (*)
ΔMPS-1/KVS-1 ($n = 3$)	3.4 ± 1.4	0.11 ± 0.06	0.7 ± 0.1	3.2 ± 0.8	0.37 ± 0.1	2.1 ± 0.8	13.9 ± 4.6

Channels were studied at +140 mV in on-cell patches. Using the maximum likelihood method[46], histograms were fitted to a double exponential function: $A_0+A_1\exp(-\tau_1/t) + A_2\exp(-\tau_2/t)$. The number of patches is indicated in parentheses. Asterisks indicate significant differences from the KVS-1 values (*, $P < 0.05$; **, $P < 0.02$; *t*-test).

gives rise to a protein that retains the ability to alter some KVS-1 functional attributes. This suggests that MPS-1 controls KVS-1 function through multiple, independent mechanisms and underscores the existence of structural and functional principles common to all KCNE β-subunits[7,22,26,40–42].

In silico analysis seems to exclude the existence of other MPS-1–like bifunctional proteins in the nematode's genome. The two closest *MPS-1* relatives, *C. elegans MPS-3* (13% identity, 31% similarity) and human *KCNE4* (13% identity, 27% similarity), lack the characteristic kinase signatures in their amino acid sequences, although this does not rule out the possibility that they might have other regulatory functions. A predicted *MPS-1* homolog in which the catalytic domain is conserved is found in the genome of *C. briggsae* (predicted protein *CBG02619*, 64% identity and 17% similarity). *C. elegans* and *C. briggsae* are close relatives, although they diverged evolutionarily approximately 50 million years ago. Nonetheless, the existence of an MPS-1 homolog in another species indicates that bifunctional proteins like MPS-1 may represent a potentially general mode of K^+ channel regulation in invertebrates, whereas (at present) there is no evidence that such proteins might operate in mammals.

KVS-1–MPS-1 channels contribute to the total current in the chemosensory neurons of *C. elegans*[6,26]. Our findings give rise to intriguing questions about the role of MPS-1 in the sensory apparatus of the animal, because phosphorylation-dependent changes in the magnitude of the KVS-1 K^+ current might have a significant impact on cell signaling. The ability of neurons in *C. elegans* to detect the multiple cues that the animal can distinguish[43–45] supports the notion that these cells must possess broad signaling capabilities. Our data would support a model predicting that MPS-1 activity favors cellular excitability through the controlled decrease or increase of the KVS-1 potassium current. Because K^+ fluxes act to stabilize the cell membrane potential, and MPS-1 decreases the current passed by KVS-1, the phosphorylation or dephosphorylation of this channel might have a role in the mechanisms determining sensory adaptation. Questions concerning the details of these mechanisms lie ahead and will be matter for future investigations.

METHODS

Molecular biology. MPS-1 mutants were constructed by polymerase chain reaction (PCR). KVS-1 was epitope tagged by replacing the terminal stop codon with nucleotides encoding HA residues (YPYDVPDYA-STOP). MPS-1 was tagged by inserting the c-Myc sequence (ISMEQKLISEEDLN). The constructs were subcloned into pcI-neo vector (Promega) for expression in CHO cells and into the pET-30b vector (Invitrogen) for expression in BL21 *E. coli* cells. All sequences were confirmed by automated DNA sequencing. Transcripts were quantified with spectroscopy and compared with control samples that were separated by agarose gel electrophoresis and stained with ethidium bromide.

Protein purification. MPS-1 in the pET-30b vector was transformed into the *E. coli* strain BL21(D3) pLysS. Bacteria were grown in 1 liter of LB medium at 37 °C to an OD_{580} of 550. Expression of recombinant MPS-1 was induced by the addition of 400 μM isopropyl β-D-thiogalactoside (IPTG). Cells were harvested by centrifugation, resuspended in BugBuster Protein Extraction Reagent (Novagen) with nuclease and incubated at room temperature for 10 min. After centrifugation at 16,000 rpm for 30 min, the pellet was resuspended in 50 mM Tris-HCl buffer, pH 8.0, containing 500 mM NaCl, 1% *n*-dodecyl-β-D-maltoside, 1 mM phenylmethylsulfonyl fluoride (PMSF), protease inhibitor and 10 mM imidazole. The suspension was incubated at 4 °C for 2 h and then centrifuged at 18,000 rpm for 30 min. The supernatant was loaded onto a HisBind column (Novagen) and washed with 50-mM Tris-HCl buffer, pH 8.0, 500 mM NaCl, 0.1% *n*-dodecyl-β-D-maltoside and 40 mM imidazole. Elution of the fusion protein was accomplished with 400 mM imidazole in the same Tris-HCl buffer solution. For the experiments with calf intestinal alkaline phosphatase (Roche), MPS-1 was washed in Amicon Ultra binding filters (Millipore) and resuspended in an imidazole-free solution.

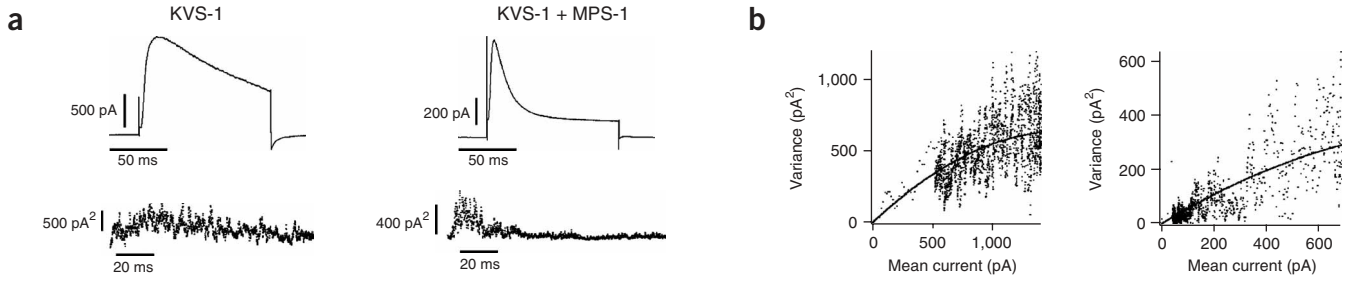

Figure 7 Fluctuation analysis of KVS-1 and KVS-1–MPS-1 channels. (**a**) Mean currents and time-dependent variances (at +60 mV) computed from 30 consecutive sweeps filtered at 5 kHz. (**b**) Mean-variance plots. Data were fitted to equation (1) as follows: $i = 0.81$ pA and $N = 3{,}000$ for the KVS-1 channels; $i = 0.70$ pA and $N = 3{,}333$ for the KVS-1–MPS-1 channels. The corresponding maximal open probability calculated from equation (2) was $p_o = 0.60$ for the KVS-1 channels and $p_o = 0.32$ for the KVS-1–MPS-1 channels.

Kinase assays. Catalytic reactions were carried out in 50 mM Tris-HCl buffer containing 50 mM NaCl, 5 mM $MgCl_2$, 1 mM DTT, 5 μCi [γ-^{32}P]ATP, 100 μM ATP, phosphatase inhibitor, ~3 μg MPS-1 and ~3 μg MBP ([γ-^{32}P]ATP was omitted in the experiments shown in **Fig. 3**). The reaction was incubated for 30 min at 37 °C and then stopped by the addition of SDS sample buffer (SDS sample buffer: 3.55 ml water, 1.25 ml 0.5 M Tris-HCl (adjusted to pH 6.8), 2.5 ml glycerol, 2.0 ml 10% (wt/vol) SDS, 0.2 ml 0.5% (wt/vol) bromophenol blue, freshly added 0.5 ml β-mercaptoethanol). Polyclonal rabbit antibodies against phosphoserine and phosphothreonine (anti-pS/pT) were purchased from Zymed. PKA from bovine heart was purchased from Sigma.

Immunoprecipitations and co-immunoprecipitations. CHO cells were washed with 10 ml ice-cold Dulbecco's phosphate-buffered saline (PBS) and lysed with ~2 ml ice-cold RIPA buffer (50 mM Tris, pH 7.4, 150 mM NaCl, 1 mM EDTA, 1% IGEPAL CA-630, 0.5% (wt/vol) deoxycholate, 0.1% (wt/vol) SDS, freshly added 10 mM iodoacetamide, phosphatase and protease inhibitors) for 30 min at 4 °C. Cell lysates were centrifuged for 60 min at 4 °C and the supernatant was mixed with HA-conjugated beads (Roche) and rocked at 4 °C for 3 h. Beads were washed three times with ice-cold TBST (Tris-buffered saline, pH adjusted to 7.6 with HCl, 0.1% Tween-20) and incubated in SDS sample buffer at ~90–95 °C for 15 min. For co-immunoprecipitations, cells were lysed with 1% Nonidet P-40 buffer, 50 mM Tris, pH 7.4, 150 mM NaCl, 1 mM EDTA, 1% IGEPAL CA-630, phosphatase and protease inhibitors (Calbiochem). Cell lysates were centrifuged for 60 min at 4 °C and the supernatant mixed with HA-conjugated beads (Roche) and rocked at 4 °C for 3 h. Beads were washed three times with ice-cold 1% Nonidet P-40 buffer and then incubated in SDS sample buffer at ~90–95 °C for 15 min.

Membrane biotinylation. At 30 h after transfection, CHO cells were washed three times with PBS at room temperature (22–25 °C) and cell surface proteins were biotinylated by 1.0 mg/ml of the impermeant biotin analog EZ-link sulfo-NHS-Lc-biotin (Pierce) in PBS. After incubation at 4 °C for 1 h, cells were washed five times with ice-cold PBS to remove any remaining biotinylation reagent. Cells were then harvested in RIPA buffer. Lysate proteins were precipitated with streptavidin-agarose beads. The precipitated KVS-1 was detected by monoclonal antibodies to HA (Roche).

Electrophysiology. CHO cells were transiently transfected with cDNA using Superfect kit (Qiagen) and studied for 24–36 h after transfection. Data were recorded with an Axopatch 200B (Axon), a PC (Dell) and Clampex software (Axon), and filtered at $f_c = 1$ kHz and sampled at 2.5 kHz (whole cell) or $f_c = 5$ kHz and sampled at 15 kHz (single-channel and noise analysis). Bath solution was (in mM): 4 KCl, 100 NaCl, 10 HEPES (pH adjusted to 7.5 with NaOH), 1.8 $CaCl_2$ and 1.0 $MgCl_2$. Pipette solution (in mM): 100 KCl, 10 HEPES (pH adjusted to 7.5 with KOH), 1.0 $MgCl_2$, 1.0 $CaCl_2$, 10 EGTA (pH adjusted to 7.5 with KOH). Addition of 2 mM magnesium ATP (Sigma) in the pipette solution had no effect on the macroscopic currents, and therefore ATP was generally omitted. Whole-cell currents were evoked by 0.1-s voltage sweeps from a holding potential of −80 mV to +120 mV, in 20-mV increments. In the experiments with staurosporine, CHO cells were preincubated for 30 min with 2 μM staurosporine (Sigma) freshly dissolved in the medium from a 2-mM stock solution (in dimethyl sulfoxide (DMSO)) and used for no longer than 30 min. During measurements, staurosporine was maintained in the bath solution at the same concentration. The concentration of DMSO in the final dilution was 0.1%, a level at which DMSO had no effect on the current (data not shown). To dialyze staurosporine from the patch pipette, we followed the procedure used with the perforated-patch technique[46]. Thus, the pipette was dipped in a standard staurosporine-free solution for ~2 s and then was back-filled with a staurosporine-containing solution. After a gigaohm seal was established, we waited for 20 min before establishing the whole-cell configuration. Voltage protocols for single-channel analysis consisted of a train of 100–300 single 2–5-s sweeps from a holding voltage of −80 mV to +120 mV, +140 mV or +160 mV. Single-channel activity was analyzed manually by pClamp 8 software (Axon). Dead time was calculated as $T_d = 0.18/f_c = 36$ μs[46]. For noise analysis, macroscopic currents were induced by 50 consecutive +60-mV depolarizing pulses from a −80-mV holding voltage in the whole cell configuration. Mean variance plots were fitted to

$$\sigma^2 = iI - \frac{I^2}{N}$$

where σ^2 is the variance, i is the unitary current, I is the macroscopic current and N is the number of channels in the cell. The maximal open probability, p_o, was calculated as:

$$p_o = \frac{I_{Max}}{Ni}$$

Throughout, statistical quantities are expressed as mean ± s.e.m.

ACKNOWLEDGMENTS

We thank L. Runnels, A. Ryazanov and J. Lenard for their comments on the manuscript and Fulvio Sesti for help with the graphics. This work was supported by grant R01GM68581-01 from the US National Institutes of Health to F.S.

COMPETING INTERESTS STATEMENT

The author declare that they have no competing financial interests.

Published online at http://www.nature.com/natureneuroscience/
Reprints and permissions information is available online at http://npg.nature.com/reprintsandpermissions/

1. MacKinnon, R. Determination of the subunit stoichiometry of a voltage-activated potassium channel. *Nature* **350**, 232–235 (1991).
2. Doyle, D. *et al.* The structure of the potassium channel: molecular bases for K^+ conduction and selectivity. *Science* **280**, 69–77 (1998).
3. Abbott, G. & Goldstein, S. A superfamily of small potassium channel subunits: form and function of the MinK-related peptides (MiRPs). *Q. Rev. Biophys.* **31**, 357–398 (1998).
4. McCrossan, Z.A. & Abbott, G.W. The MinK-related peptides. *Neuropharmacology* **47**, 787–821 (2004).
5. Wang, Y., Park, K.H., Hernandez, L., Cai, S.-Q. & Sesti, F. Biophysical and biomedical aspects of KCNE potassium channel ancillary subunits. in *Recent Research Developments in Biophysics* **Vol. 3** Part II (ed. Pandalai, S.G.) 351–363 (Transworld Research Network, Trivandrum, India, 2004).
6. Park, K.H., Hernandez, L., Cai, S.Q., Wang, Y. & Sesti, F. A Family of K+ Channel Ancillary Subunits Regulate Taste Sensitivity in *Caenorhabditis elegans*. *J. Biol. Chem.* **280**, 21893–21899 (2005).
7. Anantharam, A. *et al.* RNA interference reveals that endogenous *Xenopus* MinK-related peptides govern mammalian K^+ channel function in oocyte expression studies. *J. Biol. Chem.* **278**, 11739–11745 (2003).
8. Takumi, T., Ohkubo, H. & Nakanishi, S. Cloning of a membrane protein that induces a slow voltage-gated potassium current. *Science* **242**, 1042–1045 (1988).
9. Tai, K. & Goldstein, S. The conduction pore of a cardiac potassium channel. *Nature* **391**, 605–608 (1998).
10. Melman, Y.F., Um, S.Y., Krumerman, A., Kagan, A. & McDonald, T.V. KCNE1 binds to the KCNQ1 pore to regulate potassium channel activity. *Neuron* **42**, 927–937 (2004).
11. Chen, H., Sesti, F. & Goldstein, S.A. Pore- and state-dependent cadmium block of I(Ks) channels formed with MinK-55C and wild-type KCNQ1 subunits. *Biophys. J.* **84**, 3679–3689 (2003).
12. Sesti, F. & Goldstein, S.A. Single-channel characteristics of wild-type IKs channels and channels formed with two minK mutants that cause long QT syndrome. *J. Gen. Physiol.* **112**, 651–663 (1998).
13. Sesti, F., Tai, K.K. & Goldstein, S.A. MinK endows the I(Ks) potassium channel pore with sensitivity to internal tetraethylammonium. *Biophys. J.* **79**, 1369–1378 (2000).
14. Yang, Y. & Sigworth, F.J. Single-channel properties of IKs potassium channels. *J. Gen. Physiol.* **112**, 665–678 (1998).
15. Pusch, M. Increase of the single-channel conductance of KvLQT1 potassium channels induced by the association with minK. *Pflugers Arch.* **437**, 172–174 (1998).
16. Marx, S.O. *et al.* Requirement of a macromolecular signaling complex for beta adrenergic receptor modulation of the KCNQ1-KCNE1 potassium channel. *Science* **295**, 496–499 (2002).
17. Kurokawa, J., Chen, L. & Kass, R.S. Requirement of subunit expression for cAMP-mediated regulation of a heart potassium channel. *Proc. Natl. Acad. Sci. USA* **100**, 2122–2127 (2003).
18. McCrossan, Z.A. et al. MinK-related peptide 2 modulates Kv2.1 and Kv3.1 potassium channels in mammalian brain. *J Neurosci.* **3;23**, 8077–91 (2003).
19. Splawski, I., Tristani-Firouzi, M., Lehmann, M.H., Sanguinetti, M.C. & Keating, M.T. Mutations in the hMinK gene cause long QT syndrome and suppress IKs function. *Nat. Genet.* **17**, 338–340 (1997).
20. Piccini, M. *et al.* KCNE1-like gene is deleted in AMME contiguous gene syndrome: identification and characterization of the mouse homologues. *Genomics* **60**, 251–257 (1999).
21. Abbott, G. *et al.* MiRP2 forms potassium channels in skeletal muscle with Kv3.4 and is associated with periodic paralysis. *Cell* **104**, 217–231 (2001).
22. Abbott, G. *et al.* MiRP1 forms IKr potassium channels with HERG and is associated with cardiac arrhythmia. *Cell* **97**, 175–187 (1999).

23. Sesti, F. *et al.* A common polymorphism associated with antibiotic-induced cardiac arrhythmia. *Proc. Natl. Acad. Sci. USA* **97**, 10613–10618 (2000).
24. Splawski, I. *et al.* Spectrum of mutations in long-QT syndrome genes. KVLQT1, HERG, SCN5A, KCNE1, and KCNE2. *Circulation* **102**, 1178–1185 (2000).
25. Manning, G., Whyte, D.B., Martinez, R., Hunter, T. & Sudarsanam, S. The protein kinase complement of the human genome. *Science* **298**, 1912–1934 (2002).
26. Bianchi, L., Kwok, S.M., Driscoll, M. & Sesti, F. A potassium channel-MiRP complex controls neurosensory function in *Caenorhabditis elegans*. *J. Biol. Chem.* **278**, 12415–12424 (2003).
27. Hwang, I-S., Kim, J-H. & Choi, M-U. Kinetic study of dephosphoryltation of Myelin Basic Protein by some protein phosphates. *Bull. Korean Chem. Soc.* **18**, 428–432 (1997).
28. Miyamoto, E. & Kakiuchi, S. In vitro and in vivo phosphorylation of myelin basic protein by exogenous and endogenous adenosine 3′:5′-monophosphate-dependent protein kinases in brain. *J. Biol. Chem.* **249**, 2769–2777 (1974).
29. Laurino, J., Colca, J., Pearson, J., DeWald, D. & McDonald, J. The in vitro phosphorylation of calmodulin by the insulin receptor tyrosine kinase. *Arch. Biochem. Biophys.* **265**, 8–21 (1988).
30. Tonks, N., Diltz, C. & Fischer, E. CD45, an integral membrane protein tyrosine phosphatase. Characterization of enzyme activity. *J. Biol. Chem.* **265**, 10674–10680 (1990).
31. Ryazanova, L.V., Dorovkov, M.V., Ansari, A. & Ryazanov, A.G. Characterization of the protein kinase activity of TRPM7/ChaK1, a protein kinase fused to the transient receptor potential ion channel. *J. Biol. Chem.* **279**, 3708–3716 (2004).
32. Beeton, C.A., Chance, E.M., Foukas, L.C. & Shepherd, P.R. Comparison of the kinetic properties of the lipid- and protein-kinase activities of the p110alpha and p110beta catalytic subunits of class-Ia phosphoinositide 3-kinases. *Biochem. J.* **350**, 353–359 (2000).
33. Rintamaki, E. *et al.* Phosphorylation of light-harvesting complex II and photosystem II core proteins shows different irradiance-dependent regulation in vivo. Application of phosphothreonine antibodies to analysis of thylakoid phosphoproteins. *J. Biol. Chem.* **272**, 30476–30482 (1997).
34. Zheng, B. *et al.* The mPer2 gene encodes a functional component of the mammalian circadian clock. *Nature* **400**, 169–173 (1999).
35. Du, P. *et al.* Phosphorylation of serine residues in histidine-tag sequences attached to recombinant protein kinases: a cause of heterogeneity in mass and complications in function. *Protein Expr. Purif.* published online 7 June 2005 (doi:10.1016/j.pep.2005.04.018).
36. Sigworth, F.J. The variance of sodium current fluctuations at the node of Ranvier. *J. Physiol. (Lond.)* **307**, 97–129 (1980).
37. Ryazanov, A.G., Pavur, K.S. & Dorovkov, M.V. Alpha-kinases: a new class of protein kinases with a novel catalytic domain. *Curr. Biol.* **9**, R43–R45 (1999).
38. Runnels, L.W., Yue, L. & Clapham, D.E. TRP-PLIK, a bifunctional protein with kinase and ion channel activities. *Science* **291**, 1043–1047 (2001).
39. Drennan, D. & Ryazanov, A.G. Alpha-kinases: analysis of the family and comparison with conventional protein kinases. *Prog. Biophys. Mol. Biol.* **85**, 1–32 (2004).
40. Barhanin, J. *et al.* K(V)LQT1 and IsK (minK) proteins associate to form the I(Ks) cardiac potassium current. *Nature* **384**, 78–80 (1996).
41. Schroeder, B. *et al.* A constitutively open potassium channel formed by KCNQ1 and KCNE3. *Nature* **403**, 196–199 (2000).
42. Melman, Y.F., Domenech, A., de la Luna, S. & McDonald, T.V. Structural determinants of KvLQT1 control by the KCNE family of proteins. *J. Biol. Chem.* **276**, 6439–6444 (2001).
43. Ward, S. Chemotaxis by the nematode *Caenorhabditis elegans*: identification of attractants and analysis of the response by use of mutants. *Proc. Natl. Acad. Sci. USA* **70**, 817–821 (1973).
44. Bargmann, C. & Mori, I. in *C. elegans II* (eds. Riddle, D.L., Blumenthal, T., Meyer, B.T. & Priess, J.R.) Ch. 25 717–37 (Cold Spring Harbor Laboratory Press, Cold Spring Harbor, New York, 1997).
45. Bargmann, C.I. & Horvitz, H.R. Chemosensory neurons with overlapping functions direct chemotaxis to multiple chemicals in *C. elegans*. *Neuron* **7**, 729–742 (1991).
46. Sakmann, B. & Neher, E. (eds) *Single-Channel Recording* (Plenum Press, New York and London, 1995).